High-accuracy ^{233}U(n, f) cross-section measurement at the white-neutron source n_TOF from near-thermal to 1 MeV neutron energy

M. Calviani,[1,2,*] J. Praena,[1] U. Abbondanno,[3] G. Aerts,[4] H. Álvarez,[5] F. Álvarez-Velarde,[6] S. Andriamonje,[4] J. Andrzejewski,[7] P. Assimakopoulos,[8,†] L. Audouin,[9] G. Badurek,[10] P. Baumann,[11] F. Bečvář,[12] F. Belloni,[3,13] B. Berthier,[9] E. Berthoumieux,[4] F. Calviño,[14] D. Cano-Ott,[6] R. Capote,[15,16] C. Carrapiço,[4,17] P. Cennini,[18] V. Chepel,[19] E. Chiaveri,[18] N. Colonna,[20] G. Cortes,[21] A. Couture,[22] J. Cox,[22] M. Dahlfors,[18] S. David,[9] I. Dillmann,[23] C. Domingo-Pardo,[24] W. Dridi,[4] I. Duran,[5] C. Eleftheriadis,[25] M. Embid-Segura,[6] L. Ferrant,[9,†] A. Ferrari,[18] R. Ferreira-Marques,[19] K. Fujii,[3] W. Furman,[26] I. Goncalves,[19] E. González-Romero,[6] A. Goverdovski,[27] F. Gramegna,[1] C. Guerrero,[6] F. Gunsing,[4] B. Haas,[28] R. Haight,[29] M. Heil,[23] A. Herrera-Martinez,[18] M. Igashira,[30] E. Jericha,[10] F. Käppeler,[23] Y. Kadi,[18] D. Karadimos,[8] D. Karamanis,[8] V. Ketlerov,[27] M. Kerveno,[11] P. Koehler,[31] V. Konovalov,[27] E. Kossionides,[32] M. Krtička,[12] C. Lampoudis,[4,25] H. Leeb,[10] A. Lindote,[19] I. Lopes,[19] M. Lozano,[16] S. Lukic,[11] J. Marganiec,[7] S. Marrone,[20] T. Martínez,[6] C. Massimi,[33] P. Mastinu,[1] A. Mengoni,[15,18] P. M. Milazzo,[3] C. Moreau,[3] M. Mosconi,[23] F. Neves,[19] H. Oberhummer,[10] S. O'Brien,[22] J. Pancin,[4] C. Papachristodoulou,[8] C. Papadopoulos,[34] C. Paradela,[5] N. Patronis,[8] A. Pavlik,[35] P. Pavlopoulos,[36] L. Perrot,[4] M. T. Pigni,[10] R. Plag,[23] A. Plompen,[37] A. Plukis,[4] A. Poch,[21] C. Pretel,[21] J. Quesada,[16] T. Rauscher,[38] R. Reifarth,[29] M. Rosetti,[39] C. Rubbia,[40] G. Rudolf,[11] P. Rullhusen,[37] J. Salgado,[17] C. Santos,[17] L. Sarchiapone,[18] I. Savvidis,[25] C. Stephan,[9] G. Tagliente,[20] J. L. Tain,[24] L. Tassan-Got,[9] L. Tavora,[17] R. Terlizzi,[20] G. Vannini,[33] P. Vaz,[17] A. Ventura,[39] D. Villamarin,[6] M. C. Vincente,[6] V. Vlachoudis,[18] R. Vlastou,[34] F. Voss,[23] S. Walter,[23] M. Wiescher,[22] and K. Wisshak[23]

(n_TOF Collaboration)

^{1}*Istituto Nazionale di Fisica Nucleare, Laboratori Nazionali di Legnaro, Italy*
^{2}*Dipartimento di Fisica, Università di Padova, Italy*
^{3}*Istituto Nazionale di Fisica Nucleare, Trieste, Italy*
^{4}*CEA/Saclay—DSM/DAPNIA, Gif-sur-Yvette, France*
^{5}*Universidade de Santiago de Compostela, Spain*
^{6}*Centro de Investigaciones Energeticas Medioambientales y Tecnologicas, Madrid, Spain*
^{7}*University of Lodz, Lodz, Poland*
^{8}*University of Ioannina, Greece*
^{9}*Centre National de la Recherche Scientifique/IN2P3—IPN, Orsay, France*
^{10}*Atominstitut der Österreichischen Universitäten, Technische Universität Wien, Austria*
^{11}*Centre National de la Recherche Scientifique/IN2P3—IReS, Strasbourg, France*
^{12}*Charles University, Prague, Czech Republic*
^{13}*Università di Trieste, Italy*
^{14}*Universidad Politecnica de Madrid, Spain*
^{15}*International Atomic Energy Agency (IAEA), Nuclear Data Section, Vienna, Austria*
^{16}*Universidad de Sevilla, Spain*
^{17}*Instituto Tecnológico e Nuclear (ITN), Lisbon, Portugal*
^{18}*CERN, Geneva, Switzerland*
^{19}*LIP—Coimbra & Departamento de Fisica da Universidade de Coimbra, Portugal*
^{20}*Istituto Nazionale di Fisica Nucleare, Bari, Italy*
^{21}*Universitat Politecnica de Catalunya, Barcelona, Spain*
^{22}*University of Notre Dame, Notre Dame, Indiana 46556, USA*
^{23}*Forschungszentrum Karlsruhe GmbH (FZK), Institut für Kernphysik, Germany*
^{24}*Instituto de Física Corpuscular, CSIC—Universidad de Valencia, Spain*
^{25}*Aristotle University of Thessaloniki, Greece*
^{26}*Joint Institute for Nuclear Research, Frank Laboratory of Neutron Physics, Dubna, Russia*
^{27}*Institute of Physics and Power Engineering Obninsk, Russia*
^{28}*Centre National de la Recherche Scientifique/IN2P3—CENBG, Bordeaux, France*
^{29}*Los Alamos National Laboratory, Los Alamos, New Mexico 87545, USA*
^{30}*Tokyo Institute of Technology, Tokyo, Japan*
^{31}*Oak Ridge National Laboratory, Physics Division, Oak Ridge, Tennessee 37831, USA*
^{32}*NCSR, Athens, Greece*
^{33}*Dipartimento di Fisica, Università di Bologna, and Sezione INFN di Bologna, Italy*
^{34}*National Technical University of Athens, Greece*
^{35}*Fakultät für Physik, Universität Wien, Austria*
^{36}*Pôle Universitaire Léonard de Vinci, Paris La Défense, France*
^{37}*CEC-JRC-IRMM, Geel, Belgium*
^{38}*Department of Physics, University of Basel, Switzerland*

^{39}*ENEA, Bologna, Italy*
^{40}*Università degli Studi Pavia, Pavia, Italy*

The ^{233}U(n, f) cross section has been measured at the white neutron source n_TOF in a wide energy range with a dedicated fission ionization chamber. We report here the results from ~30 meV to 1 MeV neutron energy. The ^{233}U(n, f) cross section has been determined relative to a reference sample of ^{235}U(n, f) measured simultaneously with the same detector. The very high instantaneous neutron flux and the intrinsically low background of the n_TOF installation result in an accuracy around 3% in the whole energy range, while the energy resolution of the neutron beam allows for an accurate description of the fission cross section by means of R-matrix analysis over a wide energy range. The results are, in general, in good agreement with the most recent high-accuracy measurement of this fission cross section, over the more limited range of the previous measurements, and indicated that even the latest evaluations underestimate the cross section in the epithermal region. The present high-quality data provide the basis for a more precise evaluation of the ^{233}U fission cross section and for improving the reliability of databases needed for the design of new energy systems based on the Th/U cycle.

I. INTRODUCTION

Present concerns related, on the one hand, to the greenhouse effect and the decreasing availability of fossil fuels and, on the other hand, to the still unresolved issues of the environmental impact of nuclear energy have recently led to consider new options toward a sustainable energy supply. In the field of nuclear energy, a variety of advanced strategies are being considered for the nuclear fuel cycle and related nuclear energy systems. Different possibilities are the extension of the life span of presently operating reactors, the increase of the fuel burn-up, the plutonium recycling, and in particular the incineration of actinides and long-lived fission products in new generation reactors, which would ease waste and safety problems associated to existing nuclear energy systems. Research is being conducted on new, proliferation-resistant fuel cycles that would result in higher burn-up efficiency and lower production of high-radiotoxicity nuclear waste. In this respect, a renewed interest has recently emerged in the Th/U fuel cycle as a basis for safe and sustainable energy generation. In this cycle, the fertile element ^{232}Th is used to produce, after neutron capture and subsequent β-decays, the fissile element ^{233}U. The main advantage of the Th/U fuel cycle, as compared to the conventional U/Pu cycle, is the reduced amount of produced transuranium elements.

For the feasibility study and design of nuclear systems based on the Th/U cycle, the cross section of the basic reactions ^{232}Th(n, γ), ^{233}U(n, γ), and ^{233}U(n, f) have to be known with uncertainties of ~1–2%, ~5%, and ~1%, respectively (see, for example, Ref. [1]). However, the available experimental information is at present insufficient, and discrepancies still exist among evaluated nuclear data libraries. Therefore, new and accurate measurements, collected at innovative neutron facilities, have been requested for this important reactions to improve the reliability of cross-section data.

In this respect, high-accuracy data have been obtained at the n_TOF facility at CERN, taking advantage of the high instantaneous neutron flux, which is particularly suited for measurements on radioactive isotopes, of the very wide neutron spectrum, and of the excellent energy resolution of the neutron beam, which allows us to refine the resonance analysis up to $\simeq$1 keV. It is important to stress that more accurate resonance data help to improve predictions of the Doppler reactivity coefficient of advanced reactor systems that use ^{233}U as fuel [2].

In addition to the interest from advanced nuclear technologies, neutron-induced fission cross sections at low energy can provide important information on nuclear properties, which constitute a fundamental input in nuclear structure and reaction models, such as, for example, the level density at the neutron binding energy, that can be obtained directly from high-resolution neutron resonance spectroscopy.

In this article we report the cross section of the ^{233}U(n, f) reaction measured at n_TOF with a high-performance fission chamber in the energy region from ~30 meV to 1 MeV (for the sake of simplicity we will refer to the lower energy limit as "thermal"). In Sec. II, the experimental procedure followed in the measurement is described, while Sec. III is devoted to the data-analysis procedure. The extracted cross section is reported in Sec. IV, together with the R-matrix analysis of fission resonances, performed in the Reich-Moore approximation by using the Bayesian code SAMMY [3].

II. EXPERIMENTAL SET-UP

A. The n_TOF neutron beam

The n_TOF neutron beam is produced by spallation of 20 GeV/c protons from the CERN proton synchrotron (PS) incident on a ^{nat}Pb target. The target is cooled with a 5.8-cm-thick water layer, which acts also as moderator. The technical features of the facility and the characteristics of the neutron beam are described in detail in Ref. [4].

The most important characteristics of the n_TOF neutron beam are the very high instantaneous neutron flux

*Corresponding author: marco.calviani@cern.ch
†Deceased.

(10^5 n/cm^2/pulse at 200 m), which results in a large reduction of the background related to the natural radioactivity of the sample, and the low ambient background achieved with several massive concrete and iron shielding walls placed along the flight path. Further advantages are the high resolution in neutron energy, which allows us to improve the description of the fission cross section in terms of resonance parameters over a broad energy range, the low repetition rate of the pulsed proton beam of ⩽0.4 Hz, which eliminates the problem of bunch overlap, and the wide energy spectrum of the n_TOF neutron beam, which extends from thermal to several hundreds of MeV. The latter feature is particularly important in fission measurements: (i) it allows one to measure the cross sections even at very high energy, where only few data exist, and (ii) systematic uncertainties can be reduced, for example, by normalization to a cross-section standard at a certain energy.

The measuring station is located at a distance of 185 m from the target. Two collimators at 137 and 175 m are used for shaping the neutron beam. The beam dimensions in the experimental area are defined by the second collimator. A small aperture 1.9 cm in diameter is optional for capture cross-section measurements, while a wider aperture 8 cm in diameter is better suited for fission measurements, such as in the present case, where only very thin samples can be used.

B. Detector and data acquisition

The present measurement was performed with a fission ionization chamber (FIC), specifically built for fission cross-section measurements on radioactive U isotopes and other actinides at n_TOF. The detector and its performance are described in detail in Ref. [5]. It consists of a stack of ionization chambers, assembled along the direction of the neutron beam, thus allowing the simultaneous measurement on several isotopes. The chambers are mounted in a common pressure vessel nearly 60 cm in length. Each fission chamber consists of three electrodes: the central, 100-μm-thick Al cathode is plated on both sides with the sample material, while two 15-μm-thick Al anode foils at a distance of 5 mm from the cathode are used to define the electric field. The detector is operated with a gas mixture of 90% Ar and 10% CF$_4$ at 720 mbar pressure. The electrodes are 12 cm in diameter, while the diameter of the sample deposit is 8 cm to match the neutron beam. The detector, which was also to be used for some other actinides, was constructed to comply with the ISO 2919 norm for sealed sources [6]. The chamber was mounted in the n_TOF experimental area, at 187 m from the spallation target. In all n_TOF measurements with the FIC, reference samples of ^{235}U and/or ^{238}U were used as fission cross section standards.

The absence of the Frisch grid in the chamber and the use of specifically designed front-end electronics resulted in a fast signal with good timing properties (50 ns rise and 120 ns fall time). This feature is important to manage the pile-up problem, which is the consequence of the very high instantaneous neutron flux at n_TOF, and the background due to the high α-decay rate of the samples under investigation (in particular for the actinides).

TABLE I. Samples used in the ^{233}U(n, f) measurement. The mass is related only to the U isotopes.

Sample	Chemical form	Mass (mg)	Areal density (10^{-7} atoms/b)	Uncertainty (%)
^{235}U	U$_3$O$_8$	15.2	7.75	1.4
^{235}U	U$_3$O$_8$	16.6	8.46	1.3
^{233}U	U$_3$O$_8$	8.04	4.13	1.2
^{233}U	U$_3$O$_8$	7.45	3.83	1.2
^{233}U	U$_3$O$_8$	7.49	3.85	1.3
^{233}U	U$_3$O$_8$	7.86	4.04	1.1

The signals from the FIC were recorded with the standard n_TOF data acquisition system based on 8-bit fast flash ADCs [7] with sampling rates up to 2 GS/s and a buffer memory of 8 MB. Given the time characteristics of the FIC signals, a sampling rate of 100 MHz was chosen to obtain a reasonable number of samples per signal and to extend the time-of-flight (TOF) range to 80 ms, corresponding to a minimum neutron energy of ≈30 meV. The start for TOF measurement was provided by the so-called prompt flash, generated by ultrarelativistic particles such as electrons, muons, and γ rays produced by the interaction of the proton beam inside the spallation target.

C. The samples

In the present measurements, four ^{233}U and two ^{235}U samples were used (Table I). The samples were prepared as thin U$_3$O$_8$ layers by means of the painting technique [8–10]. While the total mass of the two isotopes is approximately equal, the ^{233}U layers were thinner to compensate for the higher fission cross section of this isotope. In this way, similar count-rates were obtained per detector, thus reducing the systematic uncertainties of the dead-time corrections. Pure uranium was used in the preparation of the samples, with very small contaminations of other isotopes, which were determined via α spectroscopy. The enrichment of the ^{233}U was 99.01%, with small admixtures of ^{234}U (0.74%), ^{235}U (0.23%), and ^{238}U (0.04%), while that of ^{235}U was 99.992%, with contribution from ^{234}U (0.02‰), ^{236}U (0.04‰), and ^{238}U (0.02‰).

III. DATA ANALYSIS

The FIC signals were analyzed off-line to extract the TOF and the energy deposited in the detector event per event. A routine based on the CERN library ROOT [5] was used to determine the TOF at peak maximum as well as baseline, amplitude, and total area of the recorded signals. In this first step, a very low threshold has been chosen to avoid that fission events with a small energy deposit in the FIC were rejected. Figure 1 shows the pulse height spectra of the ^{235}U and ^{233}U samples, averaged over the neutron energy interval from thermal to 1 MeV. Because the higher α background of the ^{233}U sample can still be well separated from the fission fragments, a simple threshold is sufficient to discriminate the backgrounds from α decay and electronic noise.
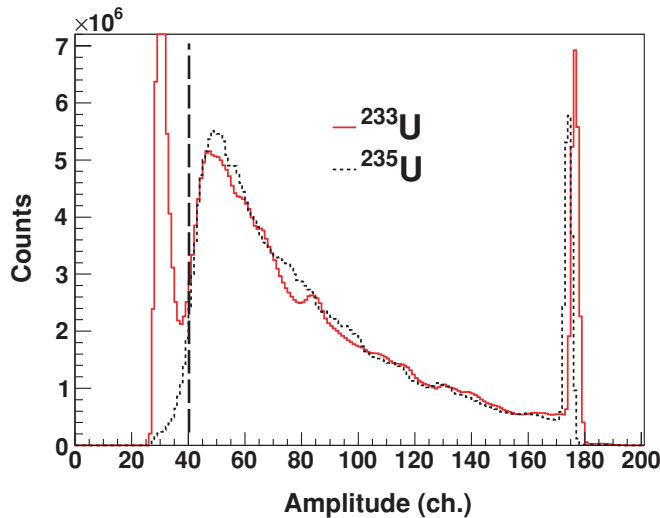
FIG. 1. (Color online) Pulse height spectra for the ^{233}U sample and for the ^{235}U reference sample. The threshold for discriminating fission fragments from α background and electronic noise is indicated by the dotted line at channel 40. The peaks observed close to channel 180 are due to a saturation effect of the flash-ADC.

For a consistent normalization between the ^{233}U and the ^{235}U reference sample, equal thresholds were applied in both spectra. The threshold, shown in Fig. 1 at channel 40 was defined to reject most of the background, while losing only a very small fraction of the fission fragments. The residual α background was checked by analyzing runs without neutron beam and was found to be negligible.

The background related to scattered neutrons, measured by means of a ^{235}U sample mounted outside the neutron beam, was found to be negligible as well. The very low overall background in the extracted cross section is demonstrated by the comparison shown in Fig. 2, where in the resonance valleys the present data are comparable, or in some cases even below, evaluated data.
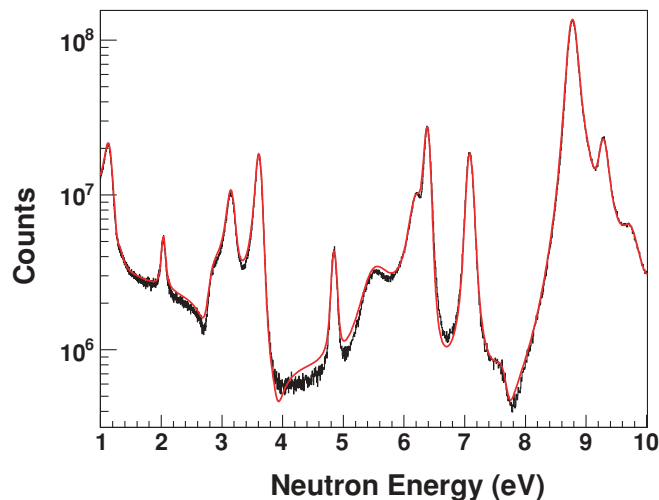

FIG. 2. (Color online) Measured ^{235}U counting rate in the energy region from 1 to 10 eV (black line), compared to the ENDF/B-VII.0 evaluation (red line), normalized at the first ^{235}U(n, f) resonance.

A. Energy calibration

The energy calibration was performed according to methods described in Ref. [11]. The effective flight path was determined by minimizing the χ^2 between the measured and tabulated energies of the ^{235}U(n, f) resonances below 600 eV [12]. The measured resonance energies were determined with a SAMMY [3] analysis of the n_TOF yield, which included the Doppler broadening and multiple scattering effects as well as the n_TOF resolution function. The extracted effective flight path is 186.95 m, which corresponds to the geometrical distance of the experimental apparatus from the surface of the Pb spallation target and the average moderation length inside the target. The additional neutron TOF term suggested in Ref. [11] to account for the moderation process was included in the calibration, although it has no significant effect in the resonance region.

B. Neutron flux and normalization

The ^{233}U(n, f) cross section is extracted according to the following expression:

$$\sigma_{33}(E_n) = \frac{C_{33}(E_n)}{N_{33} \times \Phi(E_n) \times \varepsilon_{33}}, \tag{1}$$

where C_{33} is the total number of counts of all ^{233}U samples at a given neutron energy E_n, normalized to the nominal n_TOF bunch of 7×10^{12} protons, N_{33} the total number of atoms per barn of the four ^{233}U samples, $\Phi(E_n)$ the neutron flux per proton bunch impinging on the detector, and ε the total efficiency, which varies with the energy threshold used in the event selection. The formula is valid on the assumption that the absorption of the neutron flux in the samples and in the electrodes is negligible. As shown in Ref. [5], this assumption has been verified for the present experimental setup by means of Monte Carlo simulations performed with the MCNPX code [13], which confirmed that the attenuation losses in the Al electrodes and FIC windows are of the order of a few per thousand with the exception of some very narrow regions in the keV range where the value reach $\sim$4%.

In analogy to Eq. (1) the neutron flux $\Phi(E_n)$ is determined from the respective ^{235}U(n, f) data,

$$\varepsilon_{35} \times \Phi(E_n) = \frac{C_{35}(E_n)}{N_{35} \times \sigma_{35}^{\text{eval}}(E_n)}, \tag{2}$$

Here, $\sigma_{35}^{\text{eval}}(E_n)$ represents the evaluated reference cross section, which was adopted from the ENDF/B-VII database [14].

Figure 2 shows the measured energy dependence of the number of fission events in the ^{235}U sample, normalized to the nominal bunch of 7×10^{12} protons. For comparison with the measured data, the evaluated cross section from the ENDF-B/VII database has been scaled to match the first resonance. A constant scaling factor corresponds to a flat isolethargic neutron flux distribution, which is well justified in most of the covered energy range. While excellent agreement is obtained for most resonances, some differences are obvious, particularly in the valleys between resonances. These differences, which are of the order of a few percent up to 20%, propagate to the
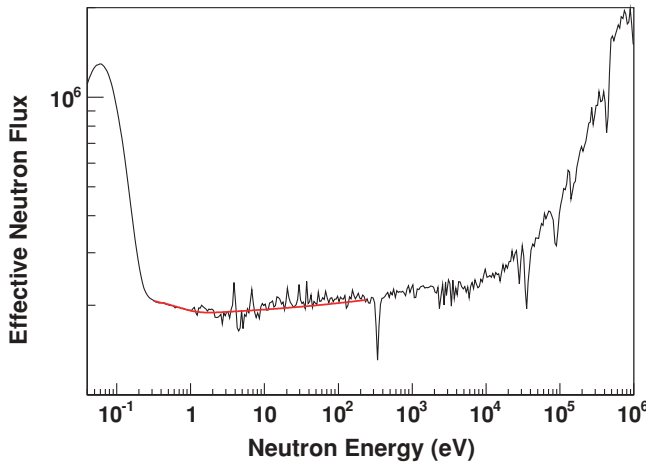
FIG. 3. (Color online) Isolethargic distribution of the effective neutron flux (i.e., the product between efficiency and neutron flux), expressed as $dn/d \ln E$ per 7×10^{12} protons and measured with the FIC detector via the ^{235}U(n, f) reaction (black histogram). The red line indicates the flux used in the present analysis between 0.16 and 245 eV, which was obtained as described in the text.

extracted neutron flux and affect, therefore, the deduced ^{233}U cross section.

Figure 3 shows the neutron flux extracted via Eq. (2) (black histogram). The artificial structures between 1 eV and ~200 eV are the direct consequence of the differences between experimental data and evaluated cross section mentioned above. To avoid these effects, the energy dependence of the neutron flux in this limited energy region was adopted from the so-called capture flux [15], measured with the small-aperture collimator used during the n_TOF capture program. Detailed data on this flux are available from measurements with the Li flux monitor [16] and with a ^{235}U loaded parallel plate fission ionization chamber from the Physikalisch-Technische Bundesanstalt at Braunschweig [17]. The red curve in Fig. 3 shows the adopted flux in the region from 0.16 to 245 eV, obtained by normalizing the "capture flux" to the one extracted via Eq. (2) between 0.16 and 1 eV. The various dips in the neutron flux correspond to absorption from O and Al resonances, either in the water moderator or in the entrance window of the neutron TOF tube. The neutron flux shown in Fig. 3 has been used to determine the ^{233}U(n, f) cross section from thermal to 10 keV.

As mentioned, the right-hand side of Eq. (2) gives the neutron flux convoluted with the FIC efficiency. However, because this is close to 100% (as shown later), the data in Fig. 3 represent the effective neutron flux in the experimental area during the fission cross-section measurements.

Above ~10 keV, i.e., in the energy region in which the ^{235}U(n, f) cross section is a smooth function of the neutron energy, the ^{233}U(n, f) cross section was determined directly from the ratio between the number of ^{233}U and ^{235}U events, using the evaluated fission cross section of ^{235}U from ENDF/B-VII.0 for normalization,

$$\sigma_{33}(E_n) = \frac{C_{33}(E_n)}{C_{35}(E_n)} \times CF \times \sigma_{35}^{\text{eval}}(E_n). \quad (3)$$

The correction factor CF includes the ratio between the number of atoms per barn in the ^{233}U and in the ^{235}U samples, as well as the efficiency and dead-time corrections described below. The use of Eq. (3) provides a more direct measurement of the ^{233}U(n, f) cross section, minimizing in particular the systematic uncertainties related to the neutron flux.

C. Efficiency and dead-time corrections

If the ^{233}U(n, f) cross section is determined relative to that of ^{235}U, one does not need to correct for the detector efficiency, provided that the same experimental and analysis conditions apply to both data sets. This was the case in the present measurement, where both ^{235}U and ^{233}U samples were measured simultaneously with the same detector and where the same analysis procedures and thresholds have been used. However, a small difference of the order of a few percent can be expected for the efficiency, because of the different thicknesses of the two samples (Table I).

The corresponding efficiency corrections were determined by detailed Monte Carlo simulations of the energy loss of the fission fragments in the sample and in the gas. In these calculations realistic mass and energy distributions for the fission fragments have been adopted from the systematics of Adeev [18].

It was assumed that the fission events were uniformly distributed inside the sample and that the fragments were emitted isotropically. The fragments were then followed in the sample and in the gas by means of the Monte Carlo simulation package FLUKA [19]. The calculated energy depositions of ^{233}U and ^{235}U fission events in the gas are plotted in Fig. 4. With the threshold used in data analysis (as shown in Fig. 1), the efficiencies are 97.1% and 93.9% for the ^{233}U and ^{235}U samples, respectively. Therefore, a correction factor of 3.3% was considered for the difference in efficiency.
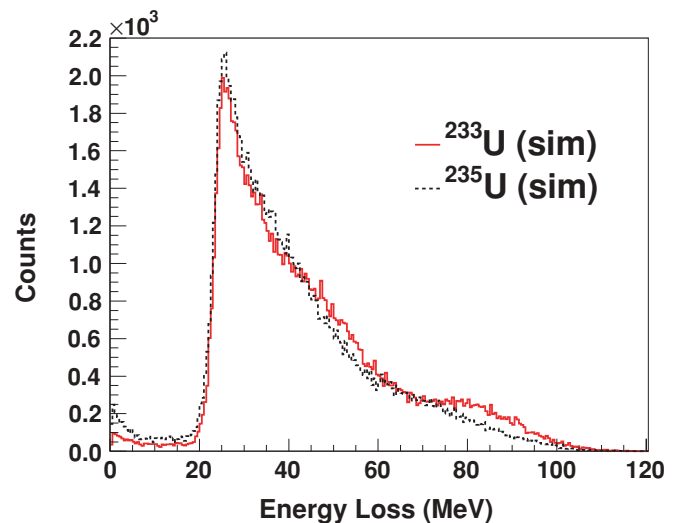

FIG. 4. (Color online) Simulated energy loss of fission fragments emitted from the ^{235}U (black histogram) and the ^{233}U samples (red histogram).

Dead-time and pile-up problems are minimized with data acquisition systems based on flash ADCs, because even overlapping signals can be identified and analyzed. However, a small dead-time effect remains because of the 230-ns minimum resolving time in the signal reconstruction routine. The corresponding correction was determined by means of a standard nonparalyzable model [20], where the instantaneous count rate was determined as a function of neutron energy for each sample and depending on the n_TOF beam conditions (dedicated or parasitic). The pile-up correction turned out to be negligible at low energy, but it becomes significant above 300 keV and reaches $\sim$10% and 12% for ^{233}U and ^{235}U, respectively, at 1 MeV. Therefore, the dead-time effect contributes less than 2% to the factor CF in Eq. (3).

D. Uncertainties

While the accurate determination of the systematic uncertainties requires a detailed analysis of the full covariance matrix, we discuss here the main sources of uncertainty and their relevance, with the aim of providing a first, conservative assessment of the accuracy of the present results.

The statistical uncertainties in the resonance region are generally smaller than 1% per data point, except in the valleys between resonances. In the keV region, the energy bins are chosen to meet this requirement. The systematic uncertainties are summarized in Table II. The uncertainty of the total mass of the ^{233}U samples, which was determined by means of α spectrometry, is 1.2%, whereas the uncertainty on the mass of the ^{235}U sample, determined also in this case by means of α spectrometry, is 1.35%. These values result in an overall contribution of 1.8% due to the mass uncertainties. The effect of possible target nonuniformities are negligible because the neutron beam profile is slightly larger than the sample diameter and almost flat in the region of the sample.

In the neutron energy region above 1 keV, where the ratio method is used, the uncertainty of the normalization procedure corresponds to that of the tabulated fission cross section of the ^{235}U standard of typically 1%. A slightly larger uncertainty of 2% has to be considered for the low-energy region ($E_n \leqslant$ 1 keV) due to the problems in the valleys between the ^{235}U(n,f) resonances as discussed before (Sec. III B). This uncertainty was estimated for the combination of the ^{235}U(n,f) data with the known n_TOF neutron flux distribution [15].

Another important uncertainty component is related to the detection efficiency, which depends essentially on the adopted pulse height threshold. Similar thresholds were chosen

TABLE II. Systematic uncertainties (in %) of the present fission cross-section data of ^{233}U.

Component	Uncertainty (%)
Sample mass	1.8
Normalization to ^{235}U(n,f)	1.0 ($\geqslant$1 keV), 2.0 ($\leqslant$1 keV)
Pulse height threshold	1.5
Dead-time correction	1.0
Total	2.7 ($\geqslant$1 keV), 3.3 ($\leqslant$1 keV)

TABLE III. The ^{233}U(n,f) cross section in the neutron energy region above 1 keV and the respective statistical uncertainties.

Energy interval (keV)	Cross section (b)	Stat. uncertainty (b)
1.002 ÷ 1.122	10.45	0.10
1.122 ÷ 1.262	10.72	0.10
1.262 ÷ 1.413	10.16	0.10
1.413 ÷ 1.589	9.65	0.10
1.589 ÷ 1.779	8.74	0.09
1.779 ÷ 2.000	8.72	0.09
2.000 ÷ 2.240	7.92	0.09
2.240 ÷ 2.518	7.89	0.09
2.518 ÷ 2820	7.43	0.08
2.820 ÷ 3.170	6.84	0.08
3.170 ÷ 3.551	6.36	0.08
3.551 ÷ 3.991	5.92	0.07
3.991 ÷ 4.470	5.66	0.07
4.470 ÷ 5.025	5.68	0.07
5.025 ÷ 5.627	5.32	0.07
5.627 ÷ 6.326	5.08	0.07
6.326 ÷ 7.084	4.65	0.06
7.084 ÷ 7.964	4.48	0.06
7.964 ÷ 8.919	4.39	0.06
8.919 ÷ 10.03	4.06	0.06
10.03 ÷ 11.23	4.12	0.06
11.23 ÷ 12.62	3.92	0.06
12.62 ÷ 14.14	3.64	0.05
14.14 ÷ 15.89	3.51	0.05
15.89 ÷ 17.80	3.49	0.05
17.80 ÷ 20.01	3.40	0.05
20.01 ÷ 22.40	3.222	0.049
22.40 ÷ 25.19	3.033	0.046
25.19 ÷ 28.20	2.928	0.046
28.20 ÷ 31.71	2.897	0.046
31.71 ÷ 35.51	2.880	0.050
35.51 ÷ 39.92	2.701	0.048
39.92 ÷ 44.70	2.562	0.041
44.70 ÷ 50.25	2.607	0.041
50.25 ÷ 56.28	2.428	0.037
56.28 ÷ 63.26	2.456	0.036
63.26 ÷ 70.84	2.501	0.037
70.84 ÷ 79.64	2.359	0.035
79.64 ÷ 89.19	2.372	0.038
89.19 ÷ 100.3	2.312	0.036
100.3 ÷ 112.3	2.237	0.032
112.3 ÷ 126.2	2.167	0.030
126.2 ÷ 141.4	2.174	0.029
141.4 ÷ 158.9	2.176	0.031
158.9 ÷ 178.0	2.162	0.029
178.0 ÷ 200.0	2.190	0.027
200.0 ÷ 224.0	2.188	0.027
224.0 ÷ 251.8	2.245	0.026
251.8 ÷ 282.0	2.224	0.025
282.0 ÷ 317.1	2.196	0.025
317.1 ÷ 355.1	2.132	0.022
355.1 ÷ 399.2	2.144	0.023
399.2 ÷ 447.0	2.061	0.024
447.0 ÷ 502.5	2.034	0.019
502.5 ÷ 562.7	1.980	0.017
562.7 ÷ 632.6	1.947	0.016

TABLE III. (*Continued.*)

Energy interval (keV)	Cross section (b)	Stat. uncertainty (b)
632.6 ÷ 708.4	1.941	0.016
708.4 ÷ 796.4	1.944	0.016
796.4 ÷ 891.9	1.917	0.016
891.9 ÷ 10.3	1.875	0.015

off-line for the ^{233}U and ^{235}U samples at half-maximum of the fission fragment amplitude distribution. The threshold could be defined within ± 1 channel in the experimental pulse height spectrum thanks to the small contribution of the α background. This threshold was used in the FLUKA simulations of the detector response, which allowed us to correct for even the small difference in detection efficiency related to the sample thickness. The final uncertainty of the pulse height threshold is 1.5%.

The dead-time corrections, which had to be considered for neutron energies above 300 keV, reached values of 10% and 12% at 1 MeV for the ^{235}U and ^{233}U samples, respectively. Because most of the dead-time corrections cancel out in the cross-section ratio, the residual correction factor is limited to only 2% at 1 MeV. Therefore, the related uncertainty is always less than 1%.

The uncertainties due to neutron beam attenuation in the samples and in the Al electrodes are of the order of a few per thousand and, therefore, negligible, except at the energies of the strongest resonances, where corrections can reach a level of 4%. Similarly, the uncertainty due to the very small divergence of the neutron beam can be neglected in view of the close spacing of the samples (1 cm).

Effects related to the angular anisotropy in the fission fragment distribution have not been included in the present data analysis, because they are small below 1 MeV [21,22] and because the FIC covers a large solid angle.

In summary, the present fission cross sections of ^{233}U in the keV region can be given with systematic uncertainties of 2.7% (Table III) and an overall uncertainty of 2.9%, whereas a systematic uncertainty of 3.3% has to be assigned to the data in the region up to 1 keV.

IV. RESULTS

A. Comparison with previous measurements

The ^{233}U(n, f) cross section has been determined at n_TOF from thermal neutron energy to 1 MeV. It is important to stress that the data are not normalized to any previous result, as in some past measurements, but rely only on the standard ^{235}U(n, f) cross section. For the first time, the whole energy range from thermal to 1 MeV is covered in a single measurement, thus minimizing possible systematic uncertainties related, for example, to the absolute normalization of the cross section.

In the following, the present results are compared with a selected set of previous data.

Figure 5 shows the low ($\leqslant 0.1$ eV) neutron energy part of the n_TOF data compared to data and evaluated libraries:
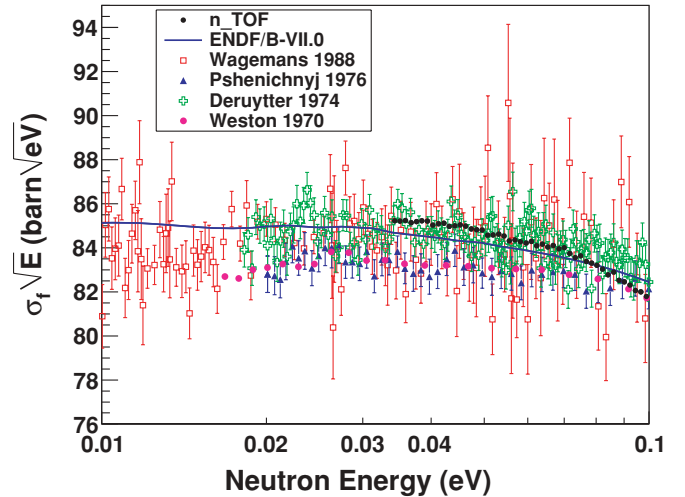

FIG. 5. (Color online) Velocity-weighted fission cross section from 10 meV to 0.1 eV. The n_TOF results (black symbols) are compared with the ENDF/B-VII.0 evaluated data (blue curve), and with previous measurements. The data of Wagemans *et al.* [23], which extends down to 2 meV, and Deruytter *et al.* [25] are normalized to the thermal ENDF/B-VI cross section of 531.14 b. The statistical uncertainties of n_TOF results are included and are as small as the symbols.

the expected flat shape of $\sigma_f(E)\sqrt{E}$ is observed close to the thermal region. Extrapolating a linear fit performed in the neutron energy range from ~ 33 to 40 meV, a value of 534.8 ± 0.2 barn is obtained for the fission cross section at thermal energy (0.0253 eV), in agreement within 1% with ENDF/B-VII.0 value of 530.70 b. This result provides an important indication of the high accuracy of the present data.

Figure 6 shows the n_TOF values (in black) in the energy region below 0.8 eV together with the evaluated cross section
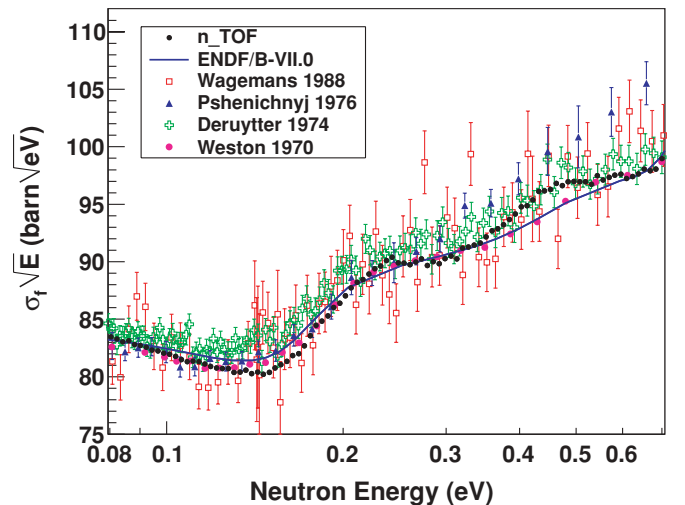

FIG. 6. (Color online) Velocity-weighted fission cross section from 0.1 to 0.8 eV. The n_TOF results (black symbols) are compared with previous measurements and with the ENDF/B-VII.0 database (blue curve). Two resonances at 0.25 and 0.45 eV are clearly observed in the n_TOF data. The statistical uncertainties of n_TOF results are included and are as small as the symbols.
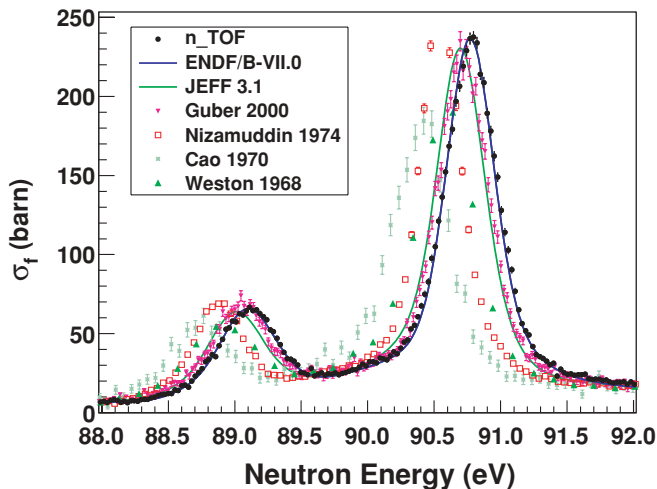
FIG. 7. (Color online) Resonances in the ^{233}U(n, f) cross section measured at n_TOF around 90 eV. Large discrepancies between previous data [30–32] and evaluations are evident. In this region, the n_TOF results confirm the evaluated data from ENDF/B-VII.0, while better agreement is observed with JEFF 3.1 in other regions. n_TOF data are given with statistical uncertainties.

FIG. 8. (Color online) The ^{233}U(n, f) cross section at the limit of the resolved resonance region in ENDF/B-VII.0. Well-resolved resonances are observed at n_TOF above this limit, in agreement with recent results of Ref. [29]. Previous results of Ref. [31] are shown for comparison.

of the ENDF/B-VII.0 database [14] and with the most recent measurements reported in EXFOR [23–26]. In general, a reasonable agreement is observed with the EXFOR data set and with the ENDF/B-VII.0 evaluation as well as with JEFF-3.1 ([27], not shown in the figure). However, the very small statistical uncertainties of the n_TOF cross section allow one to attribute the weak structures around 0.25 and 0.45 eV to low-lying resonances, which had been noted in the ENDF/B-VII.0 evaluation but had not been clearly observed in previous data. In the figures for the resonance region the n_TOF data are plotted with their statistical uncertainties, which for most of the energy region are as small as the symbols.

An example of the differences among experimental and evaluated cross-section in the resolved resonance region is shown in Fig. 7. There, the n_TOF results are compared with previous measurements and with the latest evaluations for two resonances in the energy region between 88.0 and 92.0 eV. In general, previous data exhibit sizable discrepancies, both in terms of resonance strength and energy. Correspondingly, similar differences are also found between the ENDF/B-VII.0 and JEFF-3.1 evaluations (the latter data are identical with those in the JENDL-3.3 [28] library). The n_TOF data confirm the results of Guber *et al.* [29] around 90 eV, apart from a small difference in the resonance energy. In this region the agreement with ENDF/B-VII.0 is perfect, while discrepancies exists in resonance energies with all other data [30–32], up to 0.5%, due to differences in the energy calibration and/or to a worse resolution. It should be noted that the differences observed in Fig. 7 between n_TOF data and evaluated cross section are not systematic: for some resonances JEFF-3.1 is closer to the present data that ENDF/B-VII.0, while in some other cases both libraries fail to reproduce the measured cross section.

It could be noticed from Fig. 8 that the high-energy resolution n_TOF data would allow, together with previous
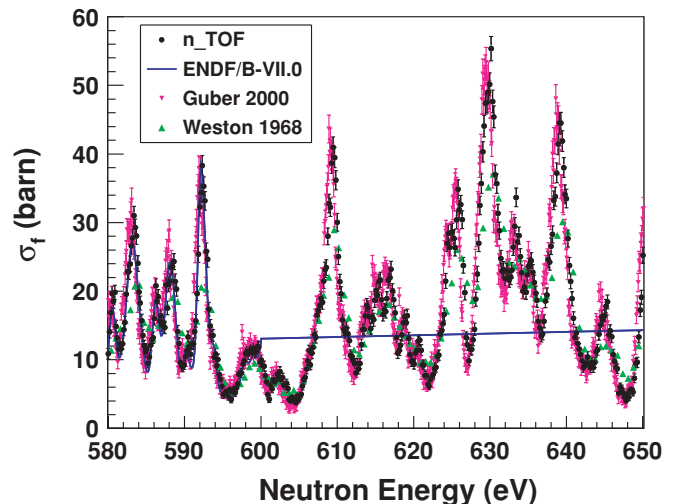
data, to extend the limit of the so-called resolved resonance region (RRR) above the current 600 eV limit of the ENDF/B-VII.0 evaluated library (in JEFF-3.1 and JENDL-3.3 resolved resonances are given only below 150 eV). Combined with the data of Guber *et al.*, the only previous measurement with comparable resolution, the n_TOF results may allow to refine the parameters related to the nuclear properties of the compound nucleus ^{234}U. Furthermore these data can be used to improve the description of the cross section in the resonance region, leading to more accurate estimates of self-shielding effects in reactor simulations [33].

The n_TOF results in the unresolved resonance region from a few tens of keV to 1 MeV are shown in Fig. 9 together with the results from previous measurements. It is important to note that some of the previous data are reported only as cross-section ratios relative to ^{235}U(n, f). For comparison with the n_TOF results, those data sets were multiplied by the ^{235}U(n, f) cross section from ENDF/B-VII.0.

Up to approximately 200 keV, the present data are mostly consistent with previous measurements. Above this energy, the previous data do not follow a common trend. In particular, the n_TOF cross section is in agreement with the measurements of Lisowski *et al.* [34], Meadows *et al.* [35], and Guber *et al.* [29] but higher than the results of Carlson *et al.* [36], Fursov *et al.* [37], and the relatively new data of Shpak *et al.* [38]. Furthermore, the evaluated cross section is about 10% lower than the n_TOF cross section.

An overview of the differences between n_TOF and existing databases is shown in Fig. 10. While the average difference between the experimental and evaluated cross sections is within 2% below 100 eV, large discrepancies exist in the region between 100 eV and 10 keV, although the evaluations are clearly too low also at higher energies. These discrepancies may well have important implications on reactor calculations aiming at establishing a Th/U fuel cycle, in particular for
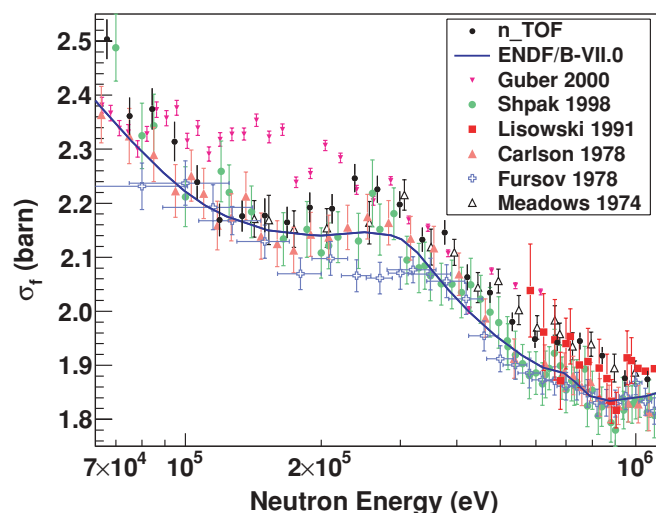
FIG. 9. (Color online) Neutron-induced fission cross section of ^{233}U measured at n_TOF between 70 keV and 1 MeV (black symbols), compared with previous results and with evaluated data from ENDF/B-VII.0. The present results confirm that the evaluated cross sections are underestimated. Data points from Ref. [29] taken from the EXFOR database have been rebinned by the authors. The bump observed in the figure for Guber's data between 100 and 250 keV is not evident in their article [29].

fast reactors. The n_TOF data strongly suggest that revised evaluations are called for, at least above 100 eV. This observation is also corroborated by the results of Guber *et al.* [29], indicating that most likely the problem is associated with a renormalization procedure performed on the evaluated cross section to account for the results of integral experiments (see Leal *et al.* [39]).

B. *R*-matrix analysis

The ^{233}U(n,f) n_TOF data are well suited for resonance analysis from thermal to 1 keV. To this purpose we have used the Bayesian code SAMMY [3] in the Reich-Moore approximation of the *R*-matrix theory. The two-fission-channels Reich-Moore formalism is used instead of the Breit-Wigner approach because the shape of the interferences of the fission channels can be reproduced with higher accuracy [39]. Corrections for the energy resolution of the neutron beam, for Doppler broadening due to thermal motion of the target nuclei, as well as for multiple scattering and self-shielding are considered in SAMMY and were taken into account in the analysis. The resolution function of the n_TOF neutron beam was also included in the fit. The Doppler broadening was modeled by a free gas at a temperature of 300K. The effect of the potential scattering was taken into account using a radius of 9.7 fm as reported in Ref. [40]. The sensitivity of the fit to variations of this parameter is very low. The background was assumed to be zero while the normalization was fixed to 1.00 and only the fission widths were left free. Only *s*-waves were considered.

The resonance parameters from thermal to 600 eV neutron energy in the ENDF/B-VII.0 library are based on the *R*-matrix resonance analysis described in Ref. [39]. We note here that, as shown in Ref. [39], the average level spacing for this nucleus is too small to allow identification of the individual resonances in the energy range above 70 eV so the observed structures are in reality aggregates of resonances (also called pseudoresonances). Nevertheless, an *R*-matrix analysis in this region is important for an accurate representation of the cross section in terms of resonance parameters. The agreement of the present experiment with the evaluated data is in general quite reasonable, but differences were found for some resonances in various energy regions. As an example, the fit of the n_TOF data between 450 and 465 eV is compared in Fig. 11 with the
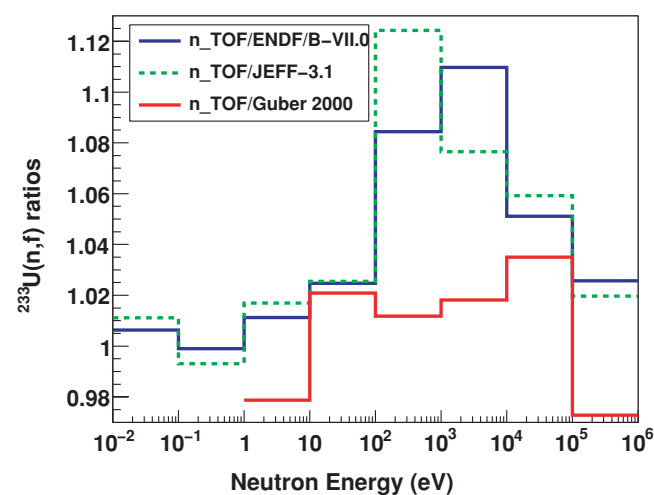

FIG. 10. (Color online) Ratio of the n_TOF results with previous data and evaluations averaged over neutron energy decades. The present results indicate a deficiency of 10% in the evaluated data between 100 eV and 10 keV, a region of interest for advanced nuclear reactor technology. The comparison between n_TOF and Guber's data in the last bin is performed up to the maximum energy of 700 keV.
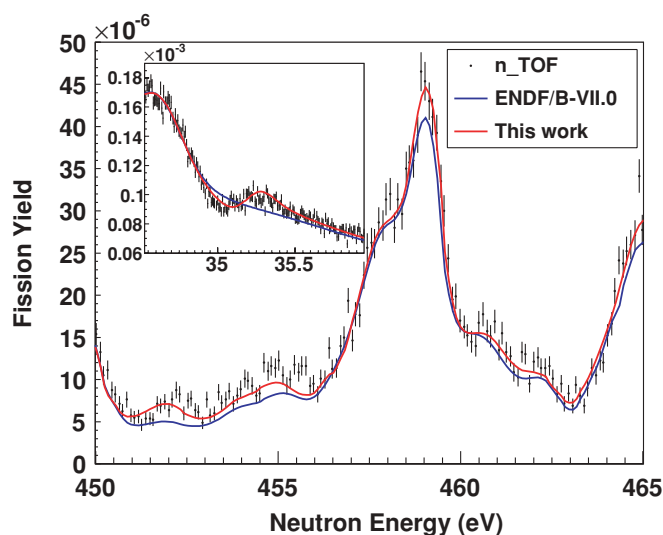

FIG. 11. (Color online) The measured and fitted n_TOF data compared with a fit based on the resonance parameters of Ref. [39] in the energy range 450 to 465 eV. The inset shows an example of a new resonance found in the present data.

reconstructed cross section from the ENDF/B-VII.0 resonance parameters.

Additionally, the inset compares a region at lower energy. With the evaluated cross section it is not possible to fit the experimental data perfectly, even if the normalization constant is left free. Similar discrepancies were also found in other energy ranges. To improve the quality of the fit, fission widths were left free in many energy ranges. New resonances were added at 35.2 and 95.04 eV (both with spin 2), thus increasing the total number of resonances from 738 to 740 [39]. Furthermore, the energies of two resonances were changed from 153.19 and 154.11 eV to 150.30 and 153.99 eV, while their spins were changed from 2 to 3, respectively. The spin change is justified by the fact that the resonance parameters depend strongly on the first guess of the spin combination, which was performed by trial-and-error, because there is no direct measurement of resonance spins [39]. With these changes we have been able to obtain a much better fit of the data in the entire ENDF/B-VII.0 RRR.

As mentioned, the energy resolution of the neutron beam allows us to observe resonances, or multiplets of resonances (pseudo-resonances), also for neutron energies above 600 eV, similarly to those observed in Ref. [29]. In a preliminary analysis from 0.6 to 1 keV about 200 pseudoresonances could be identified. Taking the recommended average spacing of 0.52 eV [39] for the mixed spin group into account implies that 569 resonances would have been missed.

As shown in Ref. [39], the performed resonance shape fits are in any case important to reproduce the structure of the experimental fission cross section to accurately evaluate the self-shielding factors and their temperature derivatives. With these motivations a preliminary fit of the structures above the current 600 eV limit of the RRR in ENDF/B-VII.0 was attempted. Figure 12 shows such a fit in the energy range between 800 and 850 eV. The spin assignments were selected from the quality of the fit via trial-and-error. A more detailed resonance analysis up to 1 keV is now being performed, taking
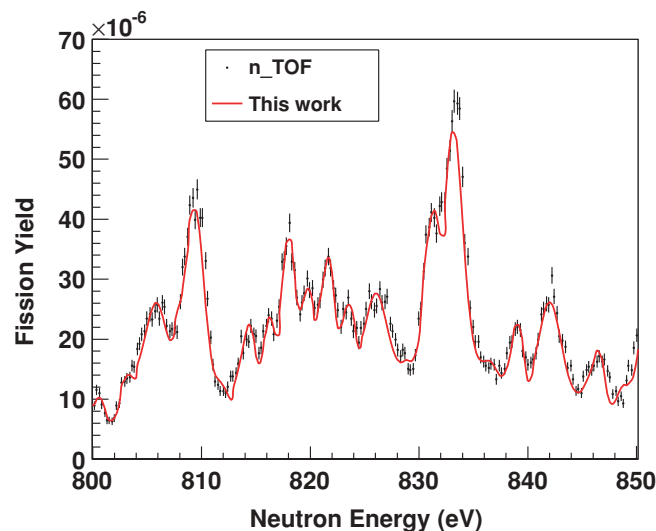
into account the low-temperature transmission experiment of Guber *et al.* [41].

While important for self-shielding calculations and their temperature derivatives in reactor physics, such an analysis may also allow us to extract or refine relevant nuclear physics parameters for this heavy nucleus, such as the behavior of the s-wave strength function and of the total fission width [39]. The detailed R-matrix analysis and its implication on the relevant nuclear physics properties will be the subject of a forthcoming publication [42].

V. SUMMARY AND CONCLUSIONS

The ^{233}U(n, f) reaction has been studied at n_TOF with a multistack fast ionization chamber from near thermal neutron energy to 1 MeV. The cross section for this reaction has been obtained relative to a ^{235}U sample, which was mounted in the same chamber and measured in the same experiment. The good discrimination between α particles and fission fragments has allowed us to apply a minimum bias in the pulse height threshold on the ^{233}U and ^{235}U spectra. Detailed simulations of the detector response have been performed to determine the difference in efficiency related to the sample thickness as well as the attenuation of the neutron beam in the electrodes and the samples.

On average, the present results show good agreement with previous data and evaluations from thermal neutron energy to 100 eV, although some differences are observed for the energy and strength of individual resonances. Important advantages of the present data are the high accuracy of the cross section (systematic uncertainties slightly above 3%), the wide energy range covered (from ∼30 meV up to 1 MeV neutron energy), and the high resolution in neutron energy, which allows us to perform an R-matrix analysis of the cross section above current limits in evaluated data libraries. A resonance shape analysis has been performed with the SAMMY code to determine the strength of the resonances. Comparison with currently available resonance parameters show sizable differences for several resonances. A more detailed resonance analysis is currently being performed.

Above 1 keV, the present results indicate that the evaluated cross section in major libraries is underestimated by as much as 12% in certain energy ranges. This finding is confirmed by another measurement performed at n_TOF with a different experimental setup [43] and is in agreement with recent data from Ref. [29]. All these observations point out to a problem even in the most recent evaluations, which can most probably be attributed to the renormalization procedure adopted to reproduce the results of integral measurements. On the basis of these results, a revision of the evaluations at least in the energy region between 100 eV and 10 keV is called for.

FIG. 12. (Color online) Preliminary R-matrix analysis of the n_TOF data in the energy range from 800 to 850 eV.

[1] INDC International Nuclear Data Committee, Tech. Rep., INDC(NDS)-408, IAEA (1999).

[2] S. Ganesan, in *Proceedings of the International Conference on Nuclear Data for Science and Technology, Santa Fe, USA, 2004*, edited by Robert Haight (Santa Fe, New Mexico, 2004), pp. 1411–1416.

[3] N. M. Larson, Tech. Rep., ORNL/TM-9179/7, 2006.

[4] U. Abbondanno *et al.*, n_TOF Performance Report, CERN/INTC-O-011, INTC-2002-037, 2002.

[5] M. Calviani *et al.*, Nucl. Instrum. Methods A **594**, 220 (2008).

[6] International Organization for Standardization, see: http://www.iso.org.

[7] U. Abbondanno *et al.*, Nucl. Instrum. Methods A **538**, 692 (2005).

[8] L. V. Drapchinsky *et al.*, Nucl. Instrum. Methods A **438**, 116 (1999).

[9] L. V. Drapchinsky *et al.*, Nucl. Instrum. Methods A **303**, 19 (1991).

[10] J. W. Behrens, Nucl. Instrum. Methods A **200**, 67 (1982).

[11] G. Lorusso *et al.*, Nucl. Instrum. Methods A **532**, 622 (2004).

[12] see: http://www-nds.iaea.org/standards.

[13] MCNPX Version 2.5.0 User's Manual, LA-CP-05-0369, April 2005.

[14] M. B. Chadwick, P. Obložinský, and M. Herman *et al.*, Nucl. Data Sheets **107**, 2931 (2006).

[15] G. Aerts *et al.* (n_TOF Collaboration), Phys. Rev. C **73**, 054610 (2006).

[16] S. Marrone *et al.*, Nucl. Instrum. Methods A **517**, 389 (2004).

[17] C. Borcea *et al.*, Nucl. Instrum. Methods A **513**, 524 (2003).

[18] G. D. Adeev *et al.*, Tech. Rep., INR Preprint 861/93, 1993.

[19] A. Fassó, A. Ferrari, J. Ranft, and P. R. Sala, Tech. Rep., CERN-2005-10, 2005; INFN/TC_05/11, SLAC-R-773, 2005.

[20] G. F. Knoll, *Radiation Detection and Measurements,* 2nd ed. (Wiley, New York, 1989).

[21] J. W. Meadows and C. Budtz-Jorgensen, in *Proceedings of the International Conference on Nuclear Data for Science and Technology, Antwerp, Belgium, 1982*, edited by K. H. Bockhoff (Reidal, Dordrecht, 1983), p. 740.

[22] D. L. Shpak *et al.*, Yad. Fiz. **61**, 1436 (1998).

[23] C. Wagemans *et al.*, in *Proceedings of the International Conference on Nuclear Data for Science and Technology, Mito, Japan, 1988*, edited by S. Igarasi (Saikon, Tokyo, 1988), p. 91.

[24] L. W. Weston *et al.*, Nucl. Sci. Eng. **42**, 143 (1970).

[25] A. J. Deruytter and C. Wagemans, Nucl. Sci. Eng. **54**, 423 (1974).

[26] V. A. Pshenichnyj *et al.*, Yaderno-Fizicheskie Issledovaniya Reports **21**, 29 (1976).

[27] The JEFF-3.1 Nuclear Data Library, JEFF Report 21, edited by A. Koning, R. Forrest, M. Kellet, R. Mills, H. Henriksson, Y. Rugama, NEA No. 6190, OECD/NEA, Paris 2006.

[28] Keiichi Shibata *et al.*, J. Nucl. Sci. Technol. **39**, 1125 (2002).

[29] K. H. Guber *et al.*, Nucl. Sci. Eng. **135**, 141 (2000), URL http://www.ans.org/pubs/journals/nse/vv-135.

[30] M. G. Cao *et al.*, J. Nucl. Energy **24**, 111 (1970).

[31] L. W. Weston *et al.*, Nucl. Sci. Eng. **34**, 1 (1968).

[32] S. Nizamuddin and J. Blons, Nucl. Sci. Eng. **54**, 116 (1974).

[33] F. B. Guimaraes, L. C. Leal, H. Derrien, and N. M. Larson, Trans. ANS **83**, 223 (2000).

[34] P. W. Lisowski *et al.*, in *Proceedings of the International Conference on Nuclear Data for Science and Technology, Juelich, Germany, 1991*, edited by S. M. Qaim (Springer Verlag, Berlin, 1992), p. 732.

[35] J. W. Meadows, Nucl. Sci. Eng. **54**, 317 (1974).

[36] G. W. Carlson and J. W. Behrens, Nucl. Sci. Eng. **66**, 205 (1978).

[37] B. I. Fursov, V. M. Kuprijanov, and G. N. Smirenking, Atomnaya Energiya **44**, 236 (1978).

[38] D. L. Shpak, Phys. At. Nucl. **61**, 1333 (1998).

[39] L. C. Leal, H. Derrien, J. A. Harvey, K. H. Guber, N. M. Larson, and R. R. Spencer, Tech. Rep. ORNL/TM-2000/372, 2001.

[40] S. F. Mughabghab, *Atlas of Neutron Resonances, Resonance Parameters and Thermal Cross Sections Z = 1–100* (Elsevier Science, Amsterdam, 2006).

[41] K. H. Guber *et al.*, Nucl. Sci. Eng. **139**, 111 (2001).

[42] J. Praena *et al.* (to be submitted to Phys. Rev. C).

[43] L. Tassan-Got *et al.* (to be submitted to Phys. Rev. C).